

# Pattern formation and the mechanics of a motor-driven filamentous system confined by cell membranes

Mitsusuke Tarama\* and Tatsuo Shibata

Laboratory for Physical Biology, RIKEN Center for Biosystems Dynamics Research, Kobe 650-0047, Japan

(Dated: September 7, 2021)

Pattern formation and the mechanics of actin filaments and myosin motors that are confined by a membrane are investigated. By using a coarse-grained molecular dynamics model, we demonstrate that the competition between depletion force and motor active force gives rise to actin accumulation in the membrane vicinity. The actomyosin structure exerts pressure on the membrane, that converges to a constant for large motor active force due to nematic alignment. The results are unaltered by filament length and membrane curvature, indicating the universality of the phenomena. Thus, this study provides a novel mechanism behind the self-organization of a motor-driven cytoskeletal network into higher-order structures.

The field of active matter has been significantly developed in recent decades. The seminal studies include the finding of the ordered state in the Vicsek model in 1995 [1] as well as the two pioneering works reported about a decade later: the theoretical study on Purcel's swimmer [2], and the experimental realization of active colloids [3–5]. Following these, a number of studies illustrated pattern formation in active matter systems in various ways [6, 7]. In addition, many studies started to focus on the rheological properties, triggered mostly by studies on suspensions of microorganisms [8, 9]. This suggests that active matter research is more than pattern formation and phase transition studies in far-from-equilibrium systems [10]. That is, the self-organized structure of active matter can serve as a basis for emergent functions. Preparing an appropriate setup enables one to extract the mechanical work from active matter [11, 12].

The mechanical functions of self-organized structures are of fundamental importance in biological systems. For instance, cells that exhibit spontaneous motion such as migration and shape deformation [13–15] coordinate their motion to heal wounds and to enable tissue morphogenesis [16–19]. Their major force-generating component is cytoskeleton, such as actin filaments and microtubules [20–25], which are themselves active matter as a result of force generation due to their associated motor proteins. They form various higher-order structures, such as the actomyosin cortex [26, 27], stress fibers [28–32], contractile rings [33, 34], and mitotic spindles [35], each of which possesses characteristic functions [36–42].

Among them, the actomyosin cortex is one of the most basic structures that maintains the cellular shape. It consists of actin filaments and myosin motors as well as other proteins that either cross-link the filaments or connect them to the membrane. These molecules accumulate in the membrane vicinity to form the actomyosin cortex. Interestingly, similar accumulation under confinement has been reported in recent studies using very simple models of active colloids [43, 44]. The phenomenon

has been compared with motility-induced phase separation [45, 46]. One of the significant differences between simple active colloids and actomyosin is that actin filaments are long filamentous molecules; about 10 nm in width and a few tens of nm to several  $\mu\text{m}$  in length with a persistence length of about 10  $\mu\text{m}$  [47]. Generally, such a long filamentous object suffers from a strong depletion force when confined, where its rotational degree of freedom is restricted. Therefore, it is non-intuitive to appreciate if actin filaments driven by myosin motors accumulate in the vicinity of a cell membrane in the absence of filament-membrane crosslinkers.

The purpose of this letter is to investigate pattern formation of an actomyosin network that interacts with a confining cell membrane and to analyze the mechanical function of the resulting self-organized structure. In particular, we focus on the competition between the depletion force and the motor active force.

We start by defining our coarse-grained molecular dynamics model of actin filaments and myosin motors. We model the filament by a linear series of discrete particles connected by elastic springs and the motor by a particle with two heads (Fig. 1a). The two motor heads can bind to two different filaments and walk actively along them. This reproduces the motion of a bipolar motor such as the non-muscle myosin II minifilaments that possess multiple actin binding sites on both ends [48]. The equations of motion for the filament and motor particles and the motor heads are given by

$$\gamma^f \frac{d\mathbf{r}_{f,i}^f}{dt} = \mathbf{f}_{f,i}^{\text{f,str}} + \mathbf{f}_{f,i}^{\text{f,bend}} + \mathbf{f}_{f,i}^{\text{f,mot}} + \mathbf{f}_{f,i}^{\text{f,memb}} + \boldsymbol{\xi}_{f,i}^f \quad (1)$$

$$\gamma^{\text{mot}} \frac{d\mathbf{r}_m^{\text{mot}}}{dt} = \sum_{h=0,1} (-\mathbf{f}_{m,h}^{\text{mot,str}} - \mathbf{f}_{m,h}^{\text{mot,bend}}) + \boldsymbol{\xi}_m^{\text{mot}} \quad (2)$$

$$\zeta r_{i(i+1)}^f \frac{d\alpha_{m,h}^{\text{mot}}}{dt} = f^{\text{walk}}. \quad (3)$$

See Supplemental Materials [49] for the derivation and detailed formulae. Here,  $\mathbf{r}_{f,i}^f$  represents the position of the  $i$ th particle of the filament  $f$ . Note the index  $f$  is omitted hereafter.  $\mathbf{r}_m^{\text{mot}}$  is the position of the motor  $m$ , and the coordinate along the filament segment

\* mitsusuke.tarama@riken.jp

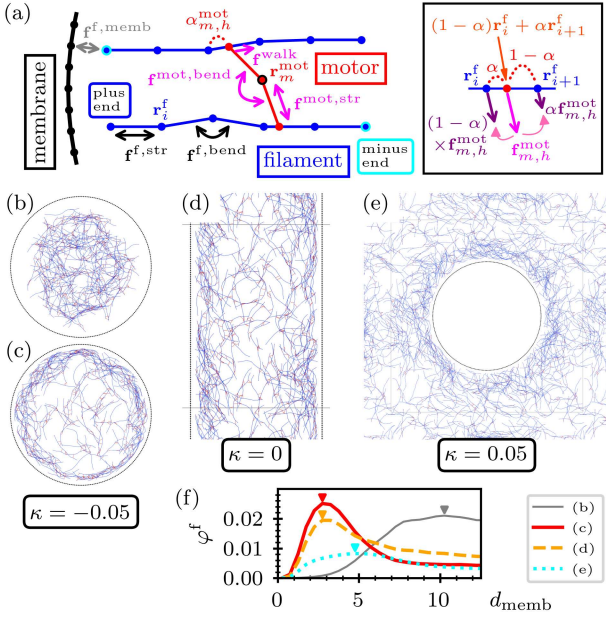


FIG. 1. (a) Schematics of the coarse-grained model of filaments and motors inside a cell membrane. The inset on the right sketches the interpolation between the filament particles, on which the motor head force is assigned using the coordinate  $\alpha$ . (b–e) Snapshots of the filaments (blue) and motors (red) confined by the membrane (black). (b) Depletion zone of the filaments of length  $L_f = 10$  is observed in the absence of motors. (c–e) Cortex-like structure is formed around the membrane with curvature (c)  $\kappa = -0.05$ , (d) 0, and (e) 0.05. The number of filaments and motors are (b–d)  $(N_f, N_m) = (200, 600)$  and (e)  $(600, 600)$ . The motor walk force (MWF) is set to  $f_{\text{walk}}^{\text{mot}} = 0$  in (b) and  $\approx 2.4$  in (c–e). In panels (d,e), thin gray lines indicate the periodic boundaries. (f) Density distribution of filaments (DDF)  $\varphi^f$  as a function of the distance from the membrane  $d_{\text{memb}}$  with its first peak position indicated by arrow heads. The cutoff distance of the filament-membrane repulsive interaction is set to  $r_{\text{cutoff}} = 1.05$ . The lines correspond to the snapshots in (b–e).

$0 \leq \alpha_{m,h}^{\text{mot}} \leq 1$  gives the  $h$ th head position of the motor  $m$  as  $(1 - \alpha_{m,h}^{\text{mot}})\mathbf{r}_i^f + \alpha_{m,h}^{\text{mot}}\mathbf{r}_{i+1}^f$  (Fig. 1a). Inertia terms are neglected because of the small size and velocity of the molecules; The typical sizes of the cytoskeletal filament and the motor are less than a few  $\mu\text{m}$  and submicrometers, respectively. The sliding velocity of the motor head is submicrometers per second. Note that the filament polarity is taken into account by the order of the filament particle indices, which gives the cue for the motor heads to walk actively towards the plus end of the filament, i.e., in increasing index  $i$ . The filament and motor particles suffer from friction and fluctuation from the surrounding cytosolic fluid, which satisfy the fluctuation-dissipation theorem;  $\langle \xi_i^X \rangle = 0$  and  $\langle \xi_{i,a}^X(0)\xi_{j,b}^X(t) \rangle = 2\gamma^X \delta_{ij} \delta_{ab} \delta(t)$  with  $X = \{f, \text{mot}\}$ . On the other hand, since the motor heads are bound to and walk along filaments due to the motor walk force (MWF)  $f_{\text{walk}}^{\text{mot}}$ , they experience a sliding friction  $\zeta r_{i(i+1)}^f d\alpha_{m,h}^{\text{mot}}/dt$ , where  $r_{i(i+1)}^f = |\mathbf{r}_{i+1}^f - \mathbf{r}_i^f|$

is the filament segment length.  $\mathbf{f}_i^{f,\text{memb}}$  is the repulsive interaction between the filament and membrane, which also confines the motors inside. The length and straightness of the filament are maintained by the stretching and bending elasticity acting between the filament particles ( $\mathbf{f}_i^{f,\text{str}}$  and  $\mathbf{f}_i^{f,\text{bend}}$ ). Similarly, the stretching and bending forces act between the motor particles and motor heads ( $\mathbf{f}_{m,h}^{\text{mot, str}}$  and  $\mathbf{f}_{m,h}^{\text{mot, bend}}$ ). Their contribution to the motor heads,  $\mathbf{f}_{m,h}^{\text{mot}} = \mathbf{f}_{m,h}^{\text{mot, str}} + \mathbf{f}_{m,h}^{\text{mot, bend}}$ , is assigned to the filament particles with the geometric weight  $\alpha_{m,h}^{\text{mot}}$ , which is necessary because the binding position may be in between the filament particles (Fig. 1a). Therefore, the force on the filament particle  $i$  from the motors reads  $\mathbf{f}_i^{f,\text{mot}} = \sum_{m,h} (1 - \alpha_{m,h}^{\text{mot}})\mathbf{f}_{m,h}^{\text{mot}} - \sum_{m,h} \alpha_{m,h}^{\text{mot}}\mathbf{f}_{m,h}^{\text{mot}}$ . Here the first and second summations are calculated over the motor heads bound to the filament segment  $\mathbf{r}_i^f - \mathbf{r}_{i+1}^f$  and  $\mathbf{r}_{i-1}^f - \mathbf{r}_i^f$ , respectively. This ensures force and torque conservation of the filament segments. Note that the counter force of the motor sliding friction and MWF, which act on the filaments, vanishes because of the force balance equation (3). Therefore, Eqs. (1)–(3) statistically satisfy the force- and torque-free conditions [49], which are required for active systems including migrating cells [14, 15].

In addition to the equations of motion (1)–(3), we consider the following stochastic processes [49]. One is filament turnover with a rate of  $\omega_{\text{TO}}^f$ . The other is the process of motor binding and unbinding. Unbinding of a motor head occurs either stochastically at the rate of  $\omega_{\text{TO}}^{\text{mot}}$  or when it reaches the end of a filament by active walking instantaneously with the probability unity. The process of motor binding to filaments causes no force on the system. The active force is applied on the cytoskeleton through the motor stretching and bending energy that are stored when motor heads move along filaments. Although this model can be applied to both actin filaments and microtubules, in this letter, we constrain ourselves to the actin filaments and myosin motors with the relevant parameters [49]. In the following, we rescale the energy, length, and time by thermal energy, motor length, and motor cytosolic friction coefficient, respectively [49].

First, we consider actomyosin dynamics inside a circular membrane. Without motors, the filaments are depleted near the membrane. This depletion zone can be observed when motors are introduced but no MWF is applied (Fig. 1b). For finite MWF, however, the filaments accumulate in the vicinity of the membrane, forming a structure that resembles the actomyosin cortex (Fig. 1c).

The question arises whether this cortex-like structure is a result of the membrane curvature. To clarify this point, we compared the results for membranes with different curvatures. Interestingly, the cortex-like structure is found at planar membranes with zero curvature as well as at a circular membrane with positive curvature, where the filaments are present outside the membrane (Figs. 1d and 1e).

To quantify this cortex-like structure, we calculated the density distribution of filaments (DDF)  $\varphi^f$  as a func-

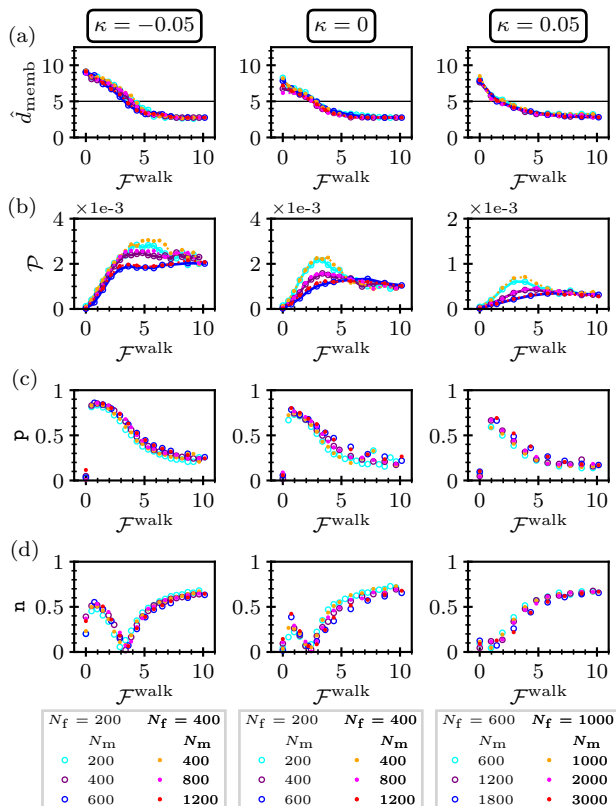


FIG. 2. Cortex-like structure formation and force generation due to MWF. (a) DDF peak distance  $\hat{d}_{\text{memb}}$  shows a good collapse as a function of the average MWF  $\mathcal{F}^{\text{walk}}$ . The black horizontal lines indicate  $L^f/2$ . (b) Scaled pressure  $\mathcal{P}$  against  $\mathcal{F}^{\text{walk}}$ . (c) Polar  $p$  and (d) nematic order parameters  $n$  of the filaments in the membrane vicinity. Each column corresponds to the membrane with curvature  $\kappa = -0.05$  (left),  $0$  (middle), and  $0.05$  (right).

tion of the distance from the membrane  $d_{\text{memb}}$  [49]. This reaches zero at the membrane and increases with  $d_{\text{memb}}$  (Fig. 1f). When MWF is absent,  $\varphi^f$  almost vanishes at small  $d_{\text{memb}}$  showing a peak at larger distance, which represents the fact that the filaments are depleted from the membrane vicinity. When MWF is switched on, however, the peak in  $\varphi^f$  appears closer to the membrane, as marked by the arrow heads. This indicates the filament accumulation in the membrane vicinity.

At equilibrium, filaments are depleted from the membrane vicinity where their rotational degrees of freedom are restricted [49]. This is also true where motors cross-link filaments but lack the active force generation (Fig. 1b). Therefore, in order for filaments to accumulate in the membrane vicinity, MWF needs to overcome the depletion force. To highlight this point, we plotted the DDF peak distance,  $\hat{d}_{\text{memb}}$ , as a function of MWF [49]. Although  $\hat{d}_{\text{memb}}$  also depends on the number of filaments and motors, we found that all data collapse on top of each other when the MWF is rescaled to the average MWF  $\mathcal{F}^{\text{walk}} = f^{\text{walk}} N_m/N_f$  (Fig. 2a). This in-

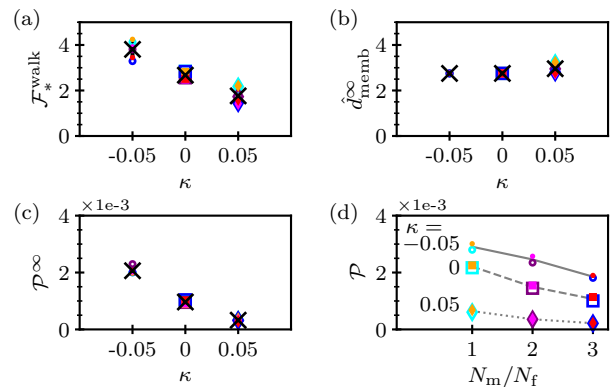


FIG. 3. Dependence of (a)  $\mathcal{F}_*^{\text{walk}}$ , (b)  $\hat{d}_{\text{memb}}^{\infty}$ , and (c)  $\mathcal{P}^{\infty}$  on the membrane curvature  $\kappa$ . The mean values plotted by the black crosses are superposed to the data for different  $N_f$  and  $N_m$ . (d) Scaled pressure  $\mathcal{P}$  against  $N_m/N_f$  for intermediate  $\mathcal{F}^{\text{walk}}$  ( $\approx 5.8$  for  $\kappa = -0.05$  and  $2.9$  for  $\kappa = 0$  and  $0.05$ ). The circle, triangle, and diamond symbols represent the data for  $\kappa = -0.05, 0$ , and  $0.05$ , and the color of each symbol corresponds to those in Fig. 2.

dicates the universality of the observed phenomena. As  $\mathcal{F}^{\text{walk}}$  increases,  $\hat{d}_{\text{memb}}$  shifts towards the membrane and becomes smaller than  $L^f/2$ , corresponding to the formation of the cortex-like structure. We define the transition point by  $\mathcal{F}^{\text{walk}} = \mathcal{F}_*^{\text{walk}}$  that gives  $\hat{d}_{\text{memb}} = L^f/2$ , at which distance the filaments basically start to experience the depletion force. Note that the critical average MWF is smaller for larger membrane curvature  $\kappa$  (Fig. 3a). Presumably this effect occurs because the rotational degree of freedom of the filaments increases with the membrane curvature, which weakens the depletion force (See Fig. S1c in [49]). In addition, we note that,  $\hat{d}_{\text{memb}}$  in the limit of large  $\mathcal{F}^{\text{walk}}$  converges to a constant value  $\hat{d}_{\text{memb}}^{\infty}$ , which is smaller than  $L^f/2$  (Fig. 3b). In conclusion, MWF exerted on the cytoskeleton acts against the depletion force, leading to the cortex-like structure formation.

Since one major function of the cytoskeleton is force generation, we measured the pressure that the actomyosin produces on the membrane as a function of MWF. The pressure depends on the number of motors and it scales with the number of filaments  $N_f$  (Figs. 2b) [49]. In fact, all the data of the scaled pressure  $\mathcal{P} = P/N_f$  collapse for small and large  $\mathcal{F}^{\text{walk}}$ . The scaled pressure converges to a constant value  $\mathcal{P}^{\infty}$  for large  $\mathcal{F}^{\text{walk}}$ . Note that  $\mathcal{P}^{\infty}$  decreases as the membrane curvature increases (Fig. 3c). For the intermediate regime of  $\mathcal{F}^{\text{walk}}$ , the value of  $\mathcal{P}$  varies depending on the number of motors, but the data collapses for each ratio  $N_m/N_f$ . Interestingly, in this regime, the scaled pressure  $\mathcal{P}$  takes *larger* value for *smaller* number of motors  $N_m/N_f$  (Fig. 3d).

To understand the reason why the DDF peak distance and the pressure on the membrane become constant for large MWF, we investigate the structural order of filaments inside the cortex-like structure. Since the symme-

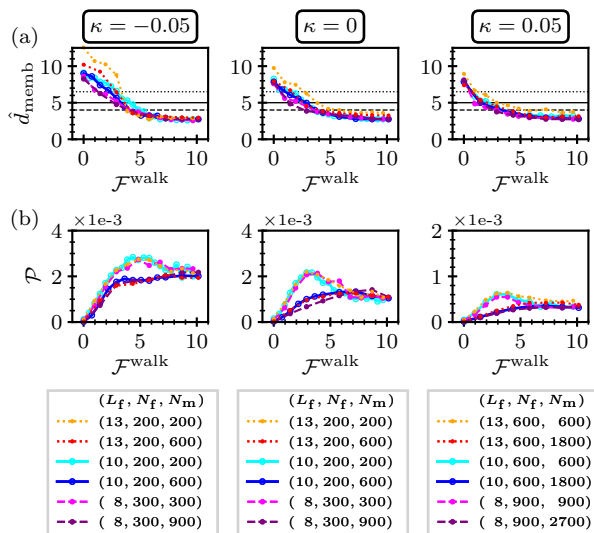


FIG. 4. Dependence of the cortex-like structure formation on the filament length. (a) DDF peak distance  $\hat{d}_{\text{memb}}$  and (b) Scaled pressure on the membrane  $\mathcal{P}$  as functions of the average MWF  $\mathcal{F}^{\text{walk}}$ . In panel (a), the dashed, solid, and dotted black lines indicate  $L_f/2$  for  $L_f = 8, 10,$  and  $13$ , respectively. Each column corresponds to the membrane with curvature  $\kappa = -0.05$  (left),  $0$  (middle), and  $0.05$  (right).

try of the system is broken by the membrane, we measure the polar and nematic order of the filaments with respect to the membrane normal direction in the membrane vicinity. We consider the relevant neighborhood  $d_{\text{memb}} \leq 1.25$ , which is about half of  $\hat{d}_{\text{memb}}^\infty$  [49]. Firstly, the magnitude of the polar order  $\mathbf{p}$  decreases as  $\mathcal{F}^{\text{walk}}$  increases (Fig. 2c), with its direction perpendicular to the membrane ( $\phi \sim 0$ ) [49]. Secondly, the nematic order  $\mathbf{n}$  increases for  $\mathcal{F}^{\text{walk}} \gtrsim \mathcal{F}_*^{\text{walk}}$  (Fig. 2d), with its direction parallel to the membrane ( $\theta \sim \pi/2$ ) [49]. These results indicate that the filaments approach the membrane as a result of MWF for  $\mathcal{F}^{\text{walk}} \lesssim \mathcal{F}_*^{\text{walk}}$ , whereas they tend to align nematicly parallel to the membrane for  $\mathcal{F}^{\text{walk}} \gtrsim \mathcal{F}_*^{\text{walk}}$ . This high nematic order of filaments aligning parallel to the membrane is the reason why  $\hat{d}_{\text{memb}}$  and  $\mathcal{P}$  converge to constant values for large  $\mathcal{F}^{\text{walk}}$  since the parallel filaments can slide along the membrane without pushing it. Further, this also explains why  $\mathcal{P}^\infty$  decreases as  $\kappa$  increases, since the filaments nematicly aligned parallel to the membrane have more chance to point away from the membrane due to fluctuation for larger membrane curvature [49]. Note that the high values of  $\mathbf{n}$  for  $\mathcal{F}^{\text{walk}} \lesssim \mathcal{F}_*^{\text{walk}}$  are induced by the high polar order  $\mathbf{p}$ , and thus both direction are the same ( $\theta \approx \phi \approx 0$ ) [49].

Finally, we study the impact of the filament length. We performed simulations with shorter ( $L_f = 8$ ) and longer ( $L_f = 13$ ) filaments than those used so far ( $L_f = 10$ ). The collapse of both the DDF peak distance  $\hat{d}_{\text{memb}}$  and the scaled pressure  $\mathcal{P}$  is unaltered by the filament length (Fig. 4). In particular, the odd increase in  $\mathcal{P}$  for smaller

motor number at intermediate  $\mathcal{F}^{\text{walk}}$  is also observed. These results are evidence of the universality in the cytoskeleton active dynamics. The structure formation is also observed for very short filaments ( $L_f \lesssim 5$ ), although the pressure profile changes, possibly because the fluctuation increases as the length decreases [49].

To summarize, we demonstrated that actomyosin accumulates in the membrane vicinity as a result of the competition between the depletion force and MWF. The self-organized cortex-like structure exerts pressure on the membrane, which converges to a constant value for large MWF because of the nematic alignment of the filaments parallel to the membrane. Interestingly, for intermediate MWF, the pressure increases when the number of motors is decreased. We highlighted the universality of the phenomena by showing the data collapse of the DDF peak position and the scaled pressure ( $\mathcal{P} = P/N_f$ ) as functions of the average MWF  $\mathcal{F}^{\text{walk}} = f^{\text{walk}} N_m/N_f$ . Qualitatively the same results are obtained for different membrane curvatures, while the critical MWF and the pressure in the large MWF limit decrease as the curvature increases. Moreover, the results are quantitatively unaltered by the filament length, except for very short filaments for which the pressure profile changes. In this case, the cortex-like structure formation is still observed. Therefore, our results provide a novel insight into the self-organization of cytoskeleton active matter into higher-order structures and the emergent mechanical functions that occur because of the structure formation.

Our model is relatively simple, such that our findings can potentially be tested against experiments on artificial cells [50, 51]. However, to our knowledge, experiments on the self-organization of actomyosin cortex in artificial cells remain challenging [52].

With respect to the actomyosin cortex in the real cells, our model omits many elements. For instance, actin nucleators and severing proteins are not included, which are thought to play a major role in the cortex formation [53]. Instead, we simplified the polymerization/depolymerization processes with a stochastic turnover. As a result, the self-organized structures tend to fade away for very large turnover rates, leading to a uniform distribution of actin filaments. Recent studies reported that contraction occurs due to additional passive crosslinkers between filaments without force generating activity [54–56]. This effect also appeared in our simulation when the crosslinkers were introduced, while this could occur both near and away from the membrane (data not shown). Therefore, to recapitulate contractile actomyosin cortex in simulation, one ought to introduce motors and crosslinkers to a filamentous network that is enriched in the membrane vicinity due to membrane-associated nucleation and biased polymerization. We will discuss this point in a separate paper. Finally, while the current work assumed a fixed membrane, it would be of interest to allow deformation to see how actomyosin structure changes cell shape [57]. In addition, it would be important to investigate how the self-organized actomyosin structure re-

acts to external stimuli [36, 58]. While beyond the scope of this letter, our simple model can be modified to examine these aspects in the future.

## ACKNOWLEDGMENTS

This work was supported by the Japan Society for the Promotion of Science (JSPS) KAKENHI (19H14673) grant, RIKEN Special Doctoral Researcher (SPDR) Program, and RIKEN Incentive Research Project, as well

as by the core funding at RIKEN Center for Biosystems Dynamics Research. T.S. was supported by JSPS KAKENHI (JP19H00996) and JST CREST (JPMJCR1852). We are grateful to Yu-Chiun Wang for stimulating discussion throughout this study and constructive comments on the manuscript from a biological viewpoint. Matthew Turner and Sonja Tarama are acknowledged for productive comments on the manuscript.

M.T. designed the research with the help from T.S.; M.T. derived the model, conducted the simulation, and performed the analysis; M.T. prepared the manuscript; T.S. approved the final manuscript.

- 
- [1] T. Vicsek, A. Czirók, E. Ben-Jacob, I. Cohen, and O. Shochet, *Phys. Rev. Lett.* **75**, 1226 (1995).
  - [2] A. Najafi and R. Golestanian, *Phys. Rev. E* **69**, 062901 (2004).
  - [3] W. F. Paxton, K. C. Kistler, C. C. Olmeda, A. Sen, S. K. St. Angelo, Y. Cao, T. E. Mallouk, P. E. Lammert, and V. H. Crespi, *Journal of the American Chemical Society* **126**, 13424 (2004).
  - [4] W. F. Paxton, S. Sundararajan, T. E. Mallouk, and A. Sen, *Angewandte Chemie International Edition* **45**, 5420 (2006).
  - [5] S. J. Ebbens and J. R. Howse, *Soft Matter* **6**, 726 (2010).
  - [6] T. Vicsek and A. Zafeiris, *Physics Reports* **517**, 71 (2012).
  - [7] S. Ramaswamy, *Annual Review of Condensed Matter Physics* **1**, 323 (2010).
  - [8] A. Sokolov and I. S. Aranson, *Phys. Rev. Lett.* **103**, 148101 (2009).
  - [9] J. Gachelin, G. Miño, H. Berthet, A. Lindner, A. Rousselet, and E. Clément, *Phys. Rev. Lett.* **110**, 268103 (2013).
  - [10] G. Gompper, R. G. Winkler, T. Speck, A. Solon, C. Nardini, F. Peruani, H. Löwen, R. Golestanian, U. B. Kaupp, L. Alvarez, T. Kiørboe, E. Lauga, W. C. K. Poon, A. DeSimone, S. Muiños-Landin, A. Fischer, N. A. Söker, F. Cichos, R. Kapral, P. Gaspard, M. Ripoll, F. Sagues, A. Doostmohammadi, J. M. Yeomans, I. S. Aranson, C. Bechinger, H. Stark, C. K. Hemelrijk, F. J. Nedelec, T. Sarkar, T. Aryaksama, M. Lacroix, G. Duclos, V. Yashunsky, P. Silberzan, M. Arroyo, and S. Kale, *Journal of Physics: Condensed Matter* **32**, 193001 (2020).
  - [11] R. Di Leonardo, L. Angelani, D. Dell'Arciprete, G. Ruocco, V. Iebba, S. Schippa, M. P. Conte, F. Mecarini, F. De Angelis, and E. Di Fabrizio, *Proceedings of the National Academy of Sciences* **107**, 9541 (2010).
  - [12] A. Kaiser, A. Peshkov, A. Sokolov, B. ten Hagen, H. Löwen, and I. S. Aranson, *Phys. Rev. Lett.* **112**, 158101 (2014).
  - [13] T. Ohta, M. Tarama, and M. Sano, *Physica D: Nonlinear Phenomena* **318 - 319**, 3 (2016).
  - [14] M. Tarama and R. Yamamoto, *Journal of the Physical Society of Japan* **87**, 044803 (2018).
  - [15] M. Tarama, K. Mori, and R. Yamamoto, *Mechanochemical subcellular-element model of crawling cells* (2019), arXiv:1905.03001.
  - [16] R. Alert and X. Trepat, *Physics Today* **74**, 30 (2021).
  - [17] T. B. Saw, A. Doostmohammadi, V. Nier, L. Kocgozlu, S. Thampi, Y. Toyama, P. Marq, C. T. Lim, J. M. Yeomans, and B. Ladoux, *Nature* **544**, 212 (2017).
  - [18] J. Howard, S. W. Grill, and J. S. Bois, *Nature Reviews Molecular Cell Biology* **12**, 392 (2011).
  - [19] M. Takeda, M. M. Sami, and Y.-C. Wang, *Nature cell biology* **20**, 36 (2018).
  - [20] J. V. Small, K. Rottner, I. Kaverina, and K. I. Anderson, *Biochimica et Biophysica Acta (BBA) - Molecular Cell Research* **1404**, 271 (1998).
  - [21] E. Paluch, J. van der Gucht, and C. Sykes, *Journal of Cell Biology* **175**, 687 (2006).
  - [22] P. A. Pullarkat, P. A. Fernández, and A. Ott, *Physics Reports* **449**, 29 (2007).
  - [23] T. Lecuit, P.-F. Lenne, and E. Munro, *Annual Review of Cell and Developmental Biology* **27**, 157 (2011).
  - [24] F. Huber, J. Schnauß, S. Rönicke, P. Rauch, K. Müller, C. Fütterer, and J. Käs, *Advances in Physics* **62**, 1 (2013).
  - [25] S. Banerjee, M. L. Gardel, and U. S. Schwarz, *Annual Review of Condensed Matter Physics* **11**, 421 (2020).
  - [26] P. Chugh and E. K. Paluch, *Journal of cell science* **131** (2018).
  - [27] G. Salbreux, G. Charras, and E. Paluch, *Trends in Cell Biology* **22**, 536 (2012).
  - [28] P. Hotulainen and P. Lappalainen, *Journal of Cell Biology* **173**, 383 (2006).
  - [29] K. Burridge and C. Guilly, *Experimental Cell Research* **343**, 14 (2016).
  - [30] S. Hu, K. Dasbiswas, Z. Guo, Y.-H. Tee, V. Thiagarajan, P. Hersen, T.-L. Chew, S. A. Safran, R. Zaidel-Bar, and A. D. Bershadsky, *Nature cell biology* **19**, 133 (2017).
  - [31] L. J. Peterson, Z. Rajfur, A. S. Maddox, C. D. Freel, Y. Chen, M. Edlund, C. Otey, and K. Burridge, *Molecular Biology of the Cell* **15**, 3497 (2004).
  - [32] S. Tojkander, G. Gateva, and P. Lappalainen, *Journal of cell science* **125**, 1855 (2012).
  - [33] R. J. Pelham and F. Chang, *Nature* **419**, 82 (2002).
  - [34] F. A. Barr and U. Gruneberg, *Cell* **131**, 847 (2007).
  - [35] I. Bennabi, M.-E. Terret, and M.-H. Verlhac, *Journal of Cell Biology* **215**, 611 (2016).
  - [36] X. Trepat, L. Deng, S. S. An, D. Navajas, D. J. Tschumperlin, W. T. Gerthoffer, J. P. Butler, and J. J. Fredberg, *Nature* **447**, 592 (2007).
  - [37] E. Sackmann, F. Keber, and D. Heinrich, *Annual Review of Condensed Matter Physics* **1**, 257 (2010).

- [38] E. Abu Shah and K. Keren, *Current Opinion in Cell Biology* **25**, 550 (2013), cell adhesion and migration.
- [39] L. Blanchoin, R. Boujemaa-Paterski, C. Sykes, and J. Plastino, *Physiological Reviews* **94**, 235 (2014).
- [40] N. C. Heer and A. C. Martin, *Development* **144**, 4249 (2017).
- [41] T. M. Svitkina, *Current Opinion in Cell Biology* **54**, 1 (2018).
- [42] A. E. Carlsson, *Current Opinion in Cell Biology* **50**, 1 (2018).
- [43] F. Smallenburg and H. Löwen, *Phys. Rev. E* **92**, 032304 (2015).
- [44] J. Elgeti and G. Gompper, *EPL (Europhysics Letters)* **101**, 48003 (2013).
- [45] M. E. Cates and J. Tailleur, *Annual Review of Condensed Matter Physics* **6**, 219 (2015).
- [46] C. Bechinger, R. Di Leonardo, H. Löwen, C. Reichhardt, G. Volpe, and G. Volpe, *Rev. Mod. Phys.* **88**, 045006 (2016).
- [47] J. Mueller, G. Szep, M. Nemethova, I. de Vries, A. D. Lieber, C. Winkler, K. Kruse, J. V. Small, C. Schmeiser, K. Keren, R. Hauschild, and M. Sixt, *Cell* **171**, 188 (2017).
- [48] C. G. Vasquez, S. M. Heissler, N. Billington, J. R. Sellers, and A. C. Martin, *eLife* **5**, e20828 (2016).
- [49] See Supplemental Material at [URL will be inserted by publisher] for the derivation of the model, a summary of the parameters, and a description of the analysis schemes.
- [50] K. Takiguchi, A. Yamada, M. Negishi, Y. Tanaka-Takiguchi, and K. Yoshikawa, *Langmuir* **24**, 11323 (2008).
- [51] M. Miyazaki, M. Chiba, H. Eguchi, T. Ohki, and S. Ishiwata, *Nature cell biology* **17**, 480 (2015).
- [52] C. Kurokawa, K. Fujiwara, M. Morita, I. Kawamata, Y. Kawagishi, A. Sakai, Y. Murayama, S.-i. M. Nomura, S. Murata, M. Takinoue, and M. Yanagisawa, *Proceedings of the National Academy of Sciences* **114**, 7228 (2017).
- [53] L.-L. Pontani, J. van der Gucht, G. Salbreux, J. Heuvingh, J.-F. Joanny, and C. Sykes, *Biophysical Journal* **96**, 192 (2009).
- [54] T. Hiraiwa and G. Salbreux, *Phys. Rev. Lett.* **116**, 188101 (2016).
- [55] T. Kim, *Biomechanics and modeling in mechanobiology* **14**, 345 (2015).
- [56] J. M. Belmonte, M. Leptin, and F. Nédélec, *Molecular Systems Biology* **13**, 941 (2017).
- [57] C. Simon, R. Kusters, V. Caorsi, A. Allard, M. Abou-Ghali, J. Manzi, A. Di Cicco, D. Lévy, M. Lenz, J.-F. Joanny, *et al.*, *Nature Physics* **15**, 602 (2019).
- [58] K. Webster, W. Ng, and D. Fletcher, *Biophysical Journal* **107**, 146 (2014).
- [59] P. Valberg and H. Feldman, *Biophysical Journal* **52**, 551 (1987).
- [60] Q. Wen and P. A. Janney, *Current Opinion in Solid State and Materials Science* **15**, 177 (2011).
- [61] H. Kojima, A. Ishijima, and T. Yanagida, *Proceedings of the National Academy of Sciences* **91**, 12962 (1994).
- [62] S. Chaen, J. Inoue, and H. Sugi, *Journal of Experimental Biology* **198**, 1021 (1995).
- [63] K. Tawada and K. Sekimoto, *Biophysical Journal* **59**, 343 (1991).